Mon. Not. R. Astron. Soc. **386,** 2330–2344 (2008) doi:10.1111/j.1365-2966.2008.13214.x

A multispectral view of the periodic events in η Carinae⋆†‡§¶

A. Damineli,[1]‖ D. J. Hillier,[2] M. F. Corcoran,[3,4] O. Stahl,[5] J. H. Groh,[1] J. Arias,[8] M. Teodoro,[1] N. Morrell,[9] R. Gamen,[7] F. Gonzalez,[7] N. V. Leister,[1] H. Levato,[7] R. S. Levenhagen,[1] M. Grosso,[7] J. F. Albacete Colombo[6] and G. Wallerstein[10]

[1]*Instituto de Astronomia, Geofísica e Ciências Atmosféricas, Universidade de São Paulo, Rua do Matão 1226, Cidade Universitária, São Paulo 05508-900, Brazil*
[2]*Department of Physics and Astronomy, University of Pittsburgh, 3941 O'Hara Street, Pittsburgh, PA 15260, USA*
[3]*CRESST and X-ray Astrophysics Laboratory, NASA/GSFC, Greenbelt, MD 20771, USA*
[4] *Universities Space Research Association, 10211 Winconsin Circle, Suite 500 Columbia, MD 21044, USA*
[5]*ZAH, Landessternwarte, Königstuhl 12, D-69117 Heidelberg, Germany*
[6]*Facultad de Ciencias Astronomicas y Geofisicas de La Plata, Buenos Aires, Argentina*
[7]*Complejo Astronomico El Leoncito, Casilla de Correo 467, San Juan, Argentina*
[8]*Departamento de Fisica, Universidad de La Serena, Chile*
[9]*Las Campanas Observatory, Carnegie Observatories, Casilla 601, La Serena, Chile*
[10]*Department of Astronomy, University of Washington, Seattle, WA 98195, USA*

Accepted 2008 March 10. Received 2008 February 28; in original form 2007 November 22

ABSTRACT

A full description of the 5.5-yr low excitation events in η Carinae is presented. We show that they are not as simple and brief as previously thought, but a combination of two components. The first, the *slow variation* component, is revealed by slow changes in the ionization level of circumstellar matter across the whole cycle and is caused by gradual changes in the wind–wind collision shock-cone orientation, angular opening and gaseous content. The second, the *collapse* component, is restricted to around the minimum, and is due to a temporary global collapse of the wind–wind collision shock. High-energy photons ($E > 16$ eV) from the companion star are strongly shielded, leaving the Weigelt objects at low-ionization state for more than six months. High-energy phenomena are sensitive only to the *collapse*, low energy only to the *slow variation* and intermediate energies to both components. Simple eclipses and mechanisms effective only near periastron (e.g. shell ejection or accretion on to the secondary star) cannot account for the whole 5.5-yr cycle.

We find anti-correlated changes in the intensity and the radial velocity of P Cygni absorption profiles in Fe II λ6455 and He I λ7065 lines, indicating that the former is associated to the primary and the latter to the secondary star. We present a set of light curves representative of the whole spectrum, useful for monitoring the next event (2009 January 11).

Key words: stars: general – stars: individual: η Carinae.

1 INTRODUCTION

η Carinae is one of the most-luminous and massive stars in the Milky Way. It underwent episodes of large mass ejections in recent centuries, one of them creating the Homunculus bipolar flow with $\sim 12\,M_\odot$ (Smith et al. 2003b). It continues to lose mass at a rate of $\sim 10^{-3}\,\dot{M}\,yr^{-1}$ through a stellar wind (Hillier et al. 2001), while intervening gas and dust precludes a clear view of the central source by ground-based observations.

Ground-based spectra show a mix of narrow, broad, permitted and forbidden emission lines (Hillier & Allen 1992; Damineli et al. 1998), some of them displaying P Cygni absorption profiles. A comprehensive description of the spectrum is found in Damineli et al. (2008), hereafter Paper I, and in the references cited in that paper. The paradoxical aspect of the spectrum is the presence of lines from high- and low-energy states. On the basis of truly periodic variations in the lines, previous work was able to show that the central source is a binary star. The primary star is colder and more luminous and the invisible companion is hotter and fainter (Damineli et al. 2000).

⋆Based partially on data collected at the OPD-LNA/MCT.
†Based partially on data collected at ESO telescopes.
‡Based partially on data collected at Casleo Observatory.
§Based partially on data collected at Magellan Telescopes.
¶Based partially on data collected at CTIO.
‖E-mail: damineli@astro.iag.usp.br

A tremendous wind–wind collision (WWC) was revealed from the X-ray light curve and spectra (Corcoran 2005; Ishibashi et al. 1999; Henley et al. 2008).

High-resolution images from the ground and from space showed the existence of condensations, named Weigelt objects (Weigelt & Ebersberger 1986), that are the main source of narrow lines and of an extended stellar wind, from where broad lines are formed (Davidson et al. 1995).

Although we have a basic picture of the system, many details are not yet understood. This is because the spectrum is incredibly complex and variable. Moreover, the observational properties of variations in lines and continua have not been presented previously. Some key features, like the permitted broad emission-line He II λ4686 (Steiner & Damineli 2004) have just been discovered in this star, even if it is one of the most frequently observed in the entire sky. This line eluded detection for more than 50 yr, due to its faintness [equivalent width (EW) < 2 Å] and transient appearance just before minimum. In spite of being faint, it reveals a huge reservoir of high-energy photons. This line originates close to the central source, but the precise location and mechanism are unknown (Martin et al. 2006a; Soker & Behar 2006). Temporal variations in the lines are an important tool to understand the system, but these have not been fully explored.

Extensive studies have also been made of the variability of Hα. Davidson et al. (2005) examined the variability of *HST* STIS observations of Hα and showed that the profile did not repeat at the same phase. In particular, a flat topped Hα profile was observed during the 2003 event, but this was not seen during the 1998–99 event. Extensive UVES observations of the south-eastern lobe were also undertaken for the 2003 event (Stahl et al. 2005; Weis et al. 2005). As the light is reflected by the Homunculus, this allows the events to be observed from different directions. Reflected variability was seen, although the line profiles are different from what we see in the direction of the central star. This confirms that the event is not spherically symmetric, a property that could be interpreted as either a latitude dependent shell event or a consequence of the different viewing angles relative to the binary orbital plane. A consistent quantitative interpretation of these data set remains to be done.

In Paper I, we presented the fundamental parameters of the 5.5-yr cycle. They are the period length $P = 2022.7 \pm 1.3$ d, the phase 0 on $T_0 =$ JD 245 2819.8 (defined by the disappearance of He I λ6678 narrow component), and the high stability of the period during the last 60 yr, only understandable in a binary scenario. However, the events are not simple eclipses, and to decipher their nature we need to examine the temporal behaviour of the permitted and forbidden lines, and their associated features (broad, narrow and P Cygni components).

This paper is organized as follows. In Section 2, we present the source and quality of data; in Section 3, we present a general view where individual emission lines originate; in Section 4, we present the general framework of the binary model to interpret the data; in Section 5, we discuss the bimodal nature of the event; in Section 6, we discuss the peculiarities of the He I λ10830 line; in Section 7, we present a multispectral view of the *collapse* component; and finally, in Section 8, we set forth a general discussion and our conclusions.

2 DATA AND MEASUREMENTS

In Paper I, we described the data acquisition and measurement, so only complimentary information is given here. Most of the data were taken at the Pico dos Dias Brazilian Observatory, with additional data taken at other South American Observatories in Argentina and Chile. Spectra were normalized to the underlying stellar continuum and the measurements performed in the standard way with the IRAF package. Broad line emission profiles were separated from the narrow components and their EWs were measured by direct integration under the line profile, since their complexity prevented fitting by standard functions.

The lines reported here cover a wide range of excitation energy and lie in the optical and near-infrared (near-IR) windows. Except in the violet, the stellar continuum has signal-to-noise ratio of generally S/N > 100. Close to [Ne III] λ3868 Å the S/N is smaller than near the other spectral lines, but this line is strong enough outside the minimum to produce accurate EWs. We do not present individual measurements and their associated errors, because this would require long tables and unnecessarily pollute the plots. Instead, we display average error bars in the figures. As a general rule, errors are ∼5 per cent for EW > 1 Å and ∼50 mÅ for fainter lines. The best way to evaluate the statistical errors is by looking to the smoothness of the line intensity curves. As a matter of fact, the real uncertainties are dominated by systematic errors and these are difficult to assess. They are caused by the extreme richness of the spectrum, which makes it difficult to define the stellar continuum, and by line deblending procedures. Systematic errors are relatively unimportant in the present work, as we are looking for patterns in the temporal variability.

The spectral resolution varies from 15 to 50 km s^{-1} and, since the radial velocity is derived from integration over many pixels, the typical uncertainty is approximately one-tenth of the spectral resolution for a single pixel (better than 5 km s^{-1}) Radial velocities are in the Heliocentric reference system.

3 GENERAL INTERPRETATION OF THE SPECTRUM

The ground-based spectra utilize a relatively large aperture, and thus sample both the central star, and different emitting regions in the circumstellar envelope (e.g. the equatorial disc, the Homunculus and the Little Homunculus). The different line contributions can be readily identified. First, there are the broad wind lines (H, Si II, Fe II), arising directly from the central star, which sample a large fraction of the wind. The broad line spectrum is similar to the P Cygni star HDE 316285 (Hillier & Allen 1992; Hillier et al. 1998). Conversely, the P Cygni absorption components are only formed on our side of the wind, in the line-of-sight towards the primary star. Secondly, the broad components of He I emission lines, once thought to be related directly to the primary star, are now thought to be excited by the ultraviolet (UV) radiation of the companion (Hillier et al. 2006) and arise in the bow-shock/wind region between the two stars (Nielsen et al. 2007a). Thirdly, there are the narrow nebular lines which arise mainly in one of three Weigelt objects (Davidson et al. 1995). Forbidden lines display other components, in addition to the narrow ones, such as the blue displaced shoulders. They seem to come from an extended region around the central star. They peak at −250 km s^{-1} in close coincidence with the speed of the gas in the radio spot at ∼1.1 arcsec north-west from the central knot (Duncan, White & Lim 1997; Teodoro et al. 2007) and both emissions could be physically connected. Fourthly, *HST* observations have revealed the existence of a 'Little Homunculus' which also has its own emission spectrum (Ishibashi et al. 2003). Fifthly, there is intrinsic emission from the Homunculus and equatorial disc, recognized by their radial velocity. Sixthly, the stellar spectrum can be seen in reflection off dust within the Homunculus. Unfortunately, in ground-based spectra, the relative contributions of these components to the ob-

served spectrum may change with time, and in a manner not directly related to the binary orbit.

Hillier & Allen (1992) showed that the nebular line emitting regions suffer significantly less extinction than does the central star. Indeed Hillier et al. (2001) estimated that the visual extinction to the central star was 7 mag in 1998 March, while Verner et al. (2002) and Verner, Brhuhweiler & Gull (2005) used 0.5 mag for the visual extinction in their analysis of the Weigelt blob spectra observed in 1998 and 1999. It is this difference in visual extinction that causes the nebular spectra to be so bright, relative to the stellar spectrum, in ground-based spectra.

Recent *HST* observations have shown that the central star has brightened by a factor of 3 between 1998 and 2003.7 (Davidson et al. 1999; Martin & Koppelman 2004), and has continued to brighten up to 2006.5 (Martin, Davidson & Koppelman 2006b). Since the stellar spectrum has not undergone marked changes, the simplest explanation is that the circumstellar extinction has declined. Ground-based photometry also shows changes, although of smaller amplitude (van Genderen et al. 2006), due to dilution by 'Homunculus' emission. Because of the variable extinction and the scattered radiation in the Homunculus, the analysis of ground-based lines is complicated. During the last 25 yr, some lines in ground-based spectra have weakened. The observed changes could be due to intrinsic changes in the knot properties, changes in the primary or in the secondary star, or decreasing circumstellar extinction. The later would cause a weakening of the Weigelt nebular lines relative to the scattered stellar continuum.

In the case of He I λ10830 (Damineli et al. 1999), the EW is decreasing faster than the stellar continuum is increasing, indicating that dust destruction/dissipation is not the only cause of the variations. This result is robust, in the sense that the flux calibration is straightforward in the near-IR; 90 per cent of the energy is in the stellar continuum and the line emission comes from a well-defined central knot. For lines in the optical range, the situation is less clear, since the contrast between the central knot and the nebula is lower. In any case, during an event, extinction variations appear to be relatively small. Further, line ratios of neighbouring nebular lines can be used, limiting the effects of circumstellar extinction.

Another issue of importance is the nature of the Weigelt objects which are believed to have been ejected sometime after 1890 – either in the smaller eruption that took place around 1890 (Smith et al. 2004) or perhaps as late as the 1930's (Dorland, Currie & Hajian 2004). Given their recent origin, it would not be surprising if the Weigelt spectra were undergoing significant changes over the last 50–100 yr. The illuminating flux is decreasing as the blobs move further away from the ionizing source (ignoring possible changes in the primary and secondary stars), and the physical conditions (e.g. density and size) of the blobs is probably changing. The influence of internal dust extinction within the blobs may also be changing, as might be the differential extinction between the blobs and the central source.

The first known and convincing evidence for high-excitation lines in the spectrum of η Carinae comes from spectra taken from 1944 to 1951 by Gaviola (1953). Spectra taken in 1938 March do not clearly show He I (Humphreys & Koppelman 2005), and as discussed by Feast, Whitelock & Marang (2001), spectra taken before 1920 do not show the high-excitation lines. This could be a confirmation of the later ejection date for the Weigelt objects, or simply reflect that their properties were very different from those today. It is even possible/probable that the gas giving rise to the narrow Fe II and [Fe II] lines in the early 1900's is not the same gas giving rise to the observed emission lines today. It should be recalled that the 'Little Homunculus' was ejected around 1890 (Ishibashi et al. 2003), and presumably this ejected material had a substantial influence on the integrated observed spectrum for some time after it was ejected. In 1893 η Carinae showed an F-type absorption spectrum, with a significant blue shift ($-200\,\mathrm{km\,s^{-1}}$) of the absorption lines, probably indicating a shell ejection (Whitney 1952). That author also notes that there were marked spectral changes until 1903, while the spectrum remained relatively unchanged between 1903 and 1930.

4 THE BASIC BINARY SCENARIO

The discovery of the strict periodicity (Damineli 1996) and binarity (Damineli, Conti & Lopes 1997) did bring some order to explore the complex variations in lines and continuum. While the period length is unique, the behaviour of the light curve (time and duration of the minimum, shape of the descending and recovering branch) differs from one feature to another. Although the ultimate cause of the event is the eccentric orbit, every feature is governed by a specific mechanism with its own characteristic time-scale. In order to discuss the different possibilities, we use a binary model like the one presented by Henley et al. (2008), but only as a general framework, which is in good general agreement with the observations, although not completely accounting for all of them.

The system is composed of two massive and evolved stars in a highly eccentric orbit, the secondary companion being the main source of (hard) ionizing photons (Damineli et al. 1997). The secondary star is hotter and less luminous than the primary, and its wind is faster and less dense. The WWC generates X-rays in the walls of a shock-cone bent towards the secondary star (Ishibashi et al. 1999). Since it is more transparent than the wind of the primary star, most of the X-rays and ionizing photons escape through it. Some of the photons from the secondary star penetrate the wind of the primary star beyond the limits of the shock-cone, producing an ionized cavity to the side of the companion star. The shock-cone points almost radially away from the primary star around apastron, but it gets twisted as it approaches periastron, when the orbital speed becomes comparable to that of the primary star wind (Pittard & Corcoran 2002). The sudden drop in the X-ray flux has been attributed to the huge increase in opacity when the shock-cone opening leaves our line-of-sight and we see the WWC through the dense wind of the primary star (Corcoran 2005). If this is the case, the wind of the primary star should be porous, since during the minimum we still see a hard X-ray component with the same temperature as in the high-excitation state (Hamaguchi et al. 2007). We will show in this work that, even if the orientation of the shock-cone opening is important, it is not the only or even the most important factor to control the variability.

The observer is placed to the side of the apastron, although not necessarily aligned to the main axis of the orbit. This is consistent with several observations: (i) the He I emissions are primarily blueshifted along most of the 5.5-yr cycle; (ii) the P Cygni absorptions, which must be formed on our side of the primary star, are weak for most of the cycle, indicating that this side is more ionized than the back side (Hillier et al. 2001, 2006; Nielsen et al. 2007a); and (iii) if periastron were on our side of the system, we should see a enhancement of $N_{\rm H}$ when the secondary star reaches the opposition, which would be coincident with the middle of the high-excitation state, but which is not observed. Further, the Weigelt objects are on our side of the system and the observation that maximum excitation occurs around $\phi = 0.5$, when the column density ($N_{\rm H}$) to X-rays is low for us, indicates that the shock-cone is opened toward us during the high-excitation state. These facts exclude models in

which the periastron is to our side of the system (Abraham et al. 2005; Kashi & Soker 2007). Because of this fundamental disagreement, we will not comment on these works, even if they are in agreement with some particular aspect of the observations. In our adopted model, the secondary star is moving away from us prior to periastron passage (Damineli et al. 1997; Pittard & Corcoran 2002). We assume, as usual, that the orbital plane is more or less perpendicular to the polar axis of the Homunculus, in order that we see the binary axis from an intermediate angle (neither parallel nor perpendicular), although there is no observational constraint to the orbital inclination.

5 THE COMPOSITE MORPHOLOGY OF THE EVENT

The variability of high-excitation lines is reasonably well known around the minimum. They show a collapse in a time-scale shorter than a few weeks, followed by a minimum a few months long. The same situation is seen in X-rays and in several broad-bands in the optical and near-IR. The event, however, covers different time-scales as we look at different spectral features.

5.1 The *slow variation* component

Damineli (1996) and Damineli et al. (1999) showed that He I λ10830 varies continuously along the 5.5-yr cycle, between minimum and maximum, with no sharp transition. An even more extreme example, showing almost sinusoidal variability, was reported by Duncan & White (2003) for the radio cm light curve. Although this is relevant to understand the mechanism of the event, since it is working all along the orbit and not confined to the periastron passage, it has not received enough attention.

In Fig. 1(a), we illustrate variations in the EW of [Ar III] λ7135 (narrow component) with orbital phase for the event #10 (phase 0 on 1997.95). Unfortunately, we do not have photometry with the same spatial and time resolution to derive the line flux from EWs. The asymmetry between the fading and recovering branches of the minimum is due, in part, to changes in the level of the continuum, but other effects are involved, since the light curve at radio wavelength is also asymmetric (Duncan & White 2003). As apparent from the figure, [Ar III] λ7135 changes through the entire cycle. In order to compensate for changes in the continuum level we measured a neighbouring line that suffers little variation along the event. We refer to the narrow line components only. The companion line for [Ar III] λ7135 is [Fe II] λ7155, also displayed in Fig. 1(a). [Fe II] shows a small decrease at $\phi = 0$, but otherwise has a smooth behaviour. We normalized all line intensities and ratios to unity at $\phi = 0.4$ in order to visually compare intensity curves. The line ratio displays a much higher degree of asymmetry than before division by the neighbouring line, indicating that both lines were affected by substantial variability of the stellar continuum along cycle #10 (which started in 1997.95 and finished in 2003.49).

If the Weigelt objects were fully ionized outside the minimum, the line intensity curve would be flat in the corresponding phases, unlike what we observe. [Ar III] shows a broad maximum in the range ($\phi =$ 0.4–0.7), whether we look to the direct EW measurements or to its ratio with the neighbouring [Fe II] line. These lines are strong when excitation is high (EW ∼ 3 Å for [Ar III] and EW ∼ 10 Å for [Fe II]). It seems plausible that only a fraction of Ar and Ne in the Weigelt objects exposed to the ionizing source is ionized to the second stage. We need better data, defining a clear maximum in the line intensity curve, to make a strong point on the partial ionization. However, it is clear that we cannot no longer say that the events in η Carinae are brief episodes. This seems to be in conflict with the fact that the event as seen in high-energy phenomena, like X-rays and He II, is confined to a narrow range of phases. This apparent contradiction is due to the existence of two regimes in the events, as shown below.

The radio light curve at 3 cm (Duncan & White 2003) shows many similarities with the [Ar III] line intensity curve for event #10; continuous variability along the whole cycle, the centre of the minimum at ∼4.5 months later than $\phi = 0$ and the asymmetry of the minimum, and with the second branch recovering slower than the fading one. An important difference is that, around the minimum, the radio light curve is sinusoidal, but [Ar III] display a sudden drop followed by a flat minimum.

The other three doubly ionized lines: [Ne III] λ3868, [Fe III] λ4701 and [S III] λ6312 behave in similar way to [Ar III] λ7135. Since [S III] λ6312 was as densely sampled in time as [Ar III] λ7135, we combined the two to enhance the S/N. In the case of [S III] λ6312, we divided its intensity by that of the neighbouring Fe II λ6318 narrow line component. We then averaged the results for [Ar III] and [S III], after having normalized the curves to the unity at phase $\phi = 0.4$. The combined line intensity curve is displayed as circles in Fig. 1(b).

In order to bring more clarity to our proposed double behaviour of the event, we modelled it by a Gaussian fit, excluding points deviating more than 3σ. We call the fit the *slow variation* component.

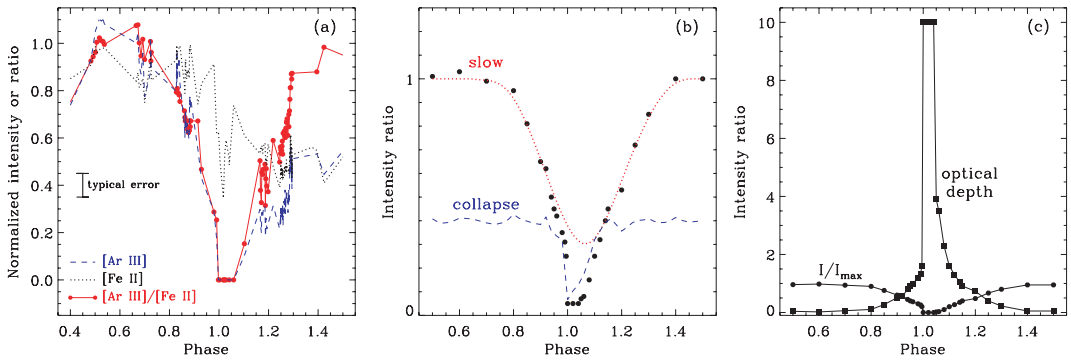

Figure 1. The *slow variation* and the *collapse* components seen in narrow lines. Panel (a): normalized EW of [Ar III] λ7135 (dashed line); [Fe II] λ7155 (dotted line); and the ratio between these two narrow line components (filled circles). A typical error bar is shown in the middle left-hand panel of the figure. Panel (b): observed intensities (circles); Gaussian fit to the 'slow' component (dotted line); and *collapse* component (dashed line) obtained by subtracting the Gaussian fit. Panel (c): EW ratios of [Ar III]/Fe II] λ7155 and [S III]/Fe II λ6318 normalized on phase $\phi = 0.4$ and averaged (I/I_{max}) (circles); optical depth (squares, see the text).

It is centred on phase $\phi = 0.069$, 140 d after $\phi = 0$ remarkably close to the radio 3-cm minimum ($\sim$130 d) and has a full width at half-maximum (FWHM) = 649 d. The Gaussian fit was subtracted from the data and the difference is represented by a dashed curve at the bottom of Fig. 1(b). We call it the *collapse* component, because of the fast drop just before $\phi = 0$ and its relation with the minimum at high energies (X-rays and He II) as discussed in the next section.

What is the cause of the slow variation changes in the doubly ionized lines? The intensity of the doubly ionized narrow lines depends on the ionizing flux the Weigelt objects receives from the secondary star. Since the binary orbit is at least 10 times smaller than its distance to the Weigelt objects, the change in the distance to the secondary star plays only a minor role in the line intensities. To get insights into the causes of the variations in the Weigelt lines, we will first interpret the radio-cm light curve, which only has a pure slow component.

Radio continuum maps (Duncan & White 2003) at 3-cm wavelengths show that the size of the radio source is maximum at $\phi = 0.5$, filling the Little Homunculus (Teodoro et al. 2007), and then shrinking to a point source as the minimum approaches. If the minimum were produced by an eclipse, in which the ionizing source is hidden from us when passing behind the primary star, or behind its stellar wind, or when the opening of the shock-cone around the secondary star leaves our line-of-sight, there would always be gas being ionized in other directions, except ours. The net effect would be a change in the small scale structure of the radio map due to irregular density distribution, but not in its size and flux density. The facts that, during the minimum, the size of the radio map is reduced to almost a point source and that the flux density decreases indicate that the volume of ionized gas in the circumstellar medium also decreases. This indicates that a fraction of ionizing photons coming the secondary star are impeded from escaping to the circumstellar environment, which implies that the size of the shock-cone opening is decreasing toward periastron and/or the gas density inside its cavity is increasing. The shock-cone is not rotating as a rigid body around the centre of mass, especially in regions far from its apex. Far from this region, the gas flow may be disturbed and left behind, in a spiral-like pattern, increasing the opacity for escaping photons. The effect may be small for X-rays but high for UV radiation. In this scenario, the radio light curve is not expected to be symmetric with respect to the periastron passage, as is observed.

We can interpret the *slow variation* component of the double excited nebula lines in the same manner as the radio light curve. In this case, variations in the line intensity of doubly ionized lines represent changes in the optical depth toward the secondary star, as seen from the Weigelt objects. In order to explore the idea that the ionization in the Weigelt objects is controlled by opacity, let us define an optical depth, by assuming that it is zero at maximum line intensity and increases in proportion to the decrease in the line intensity. For example, at 90 per cent of the maximum intensity, the optical depth is $\tau = 0.046$, and so on, as displayed in Table 1.

Table 1. Parametrization of the event for [Ar III] and [S III].

$I/I_{\max}$	Length[a] (d)	Optical depth τ
0.90	1214	0.046
0.50	587	0.30
0.10	182	1.0
0.0	120	$\gg$1

[a]Time to return to the same line intensity.

Fig. 1(c) illustrates the change in optical depth (squares) along the curve intensity of the doubly ionized lines ($I/I_{\max}$). We see that the optical depth has a smooth behaviour along the 5.5-yr cycle, as expected from the *slow variation* component, suffering a sudden increase when the optical depth reaches $\sim$1. The short-lived *collapse* component corresponds to points with $\tau > 1$.

Another way to examine the evidence for two components in the 5.5-yr cycle is by looking for how long the line intensity curve stays above some intensity or above some optical depth. As seen in Table 1, the optical depth remains at $\tau > 1$ for approximately six months close to the minimum and at $\tau < 1$ for the remaining 5 yr.

5.2 The *collapse* component

The *collapse* component derived by subtraction of the Gaussian fit is centred at $\phi = 0.0299$ (60 d after $\phi = 0$), has FWHM = 189 d and covers 30 per cent of the area under the curve. It starts when the doubly ionized forbidden lines fall below $\sim$40 per cent of their maximum intensity, and lasts for $\sim$15 per cent of the 5.5-yr cycle. We reinforce that these values are specific to [Ar III] and [S III] and other features may result in different values, since they are affected by different proportions of the *collapse* and the *slow variation* components. Moreover, these values were measured in the subtracted curve, which may be contaminated by defects in the deblending procedure.

What causes the crash in intensities in the *collapse* component? The optical depth rises steeply as $\phi = 0$ approaches. It is unlikely due to a simple eclipse, since the wind of the primary star is optically thick up to many stellar radii (Hillier et al. 2001) and has a gradual radial density profile. At this epoch, the Weigelt objects are suddenly screened from high-energy ($E > 16$ eV) ionizing radiation. A possible explanation would be that, as the shock-cone opening changes direction around the orbit, the line-of-sight from the secondary star to the Weigelt objects crosses its walls, entering into the high-opacity region dominated by the primary's wind. Let us call it the 'cone eclipse'. Interestingly, all features that have the *collapse* component (e.g. X-rays, He II λ4686, etc.) show such a fast drop. However, this does not necessarily mean that the same mechanism needs to be invoked to explain all features – instead we note that the time-scale for the collapse phase is ultimately driven by the short time the secondary spends near periastron.

The collapse in X-rays has been attributed to the 'cone eclipse' just mentioned, when our line-of-sight leaves the cone opening (Pittard & Corcoran 2002). Since the Weigelt objects do not lay on our line-of-sight and both features (X-rays and doubly ionized lines) fade simultaneously, the same explanation cannot hold for the Weigelt lines. The 'cone eclipse' could be attributed to the collapse of He II λ4686 seen directly in the central object. However, its image reflected by the dust near the Homunculus South Pole, $\sim$45° from our line-of-sight, collpases at the same time – after correcting for the extra travel time to the 'Homunculus' South Pole, (Stahl et al. 2005). In this case too the 'cone eclipse' seems implausible.

Since there are many features, formed in different places of the system, which show a synchronized fading, we suggest a simple hypothesis: the WWC shock suffers a temporary global collapse when the stars are close enough to periastron. Previous work suggested that the events in η Carinae (principally changes at the central minimum) are due to a global change in the WWC. Soker (2005), in order to explain the fast drop in the X-ray curve and the long time-scale of the minimum, advocates that near periastron the companion accretes from the primary's wind. Martin et al. (2006a) and (Davidson 2002) discussed difficulties for eclipse models to account for these

two features in the X-ray light curve, in the He II line intensity and in the radial velocity curves. These authors suggest that the radiative and tidal forces of the secondary companion star induce a major disturbance in the inner wind of the primary, resulting in a shell ejection. Alternatively, they suggest that WWC shock may become unstable because of the large density near periastron and suffer a general crash. Although our data are not useful to select any special mechanism, or a particular mechanism, we recognize that there is a sudden and simultaneous fading in many broad band light curves and spectral line intensities all over the spectrum. We call it the 'collapse' component.

5.3 A detailed view of the *collapse* component for doubly ionized lines

In this section, we explore the duration of the minimum for the doubly ionized forbidden lines and show that they disappear and re-appear in a defined sequence. Since we measured the EW of the narrow component separately, they represent the way the Weigelt objects experience the event.

During the monitoring campaign of the 2003.5 event, we noticed that when the narrow component of He I λ6678 disappeared, [Fe III] λ4701 was still detectable and that [Ne III] λ3868 had disappeared a few days earlier. In Fig. 2, we display the behaviour of [S III], [Ne III], [Ar III], and [Fe III] narrow components, measured in milli-Angstrom (mÅ). [Ne III], the highest excitation energy line among these four, is the first to disappear and the last to re-appear. [Fe III], with the lowest energy transition, fades later and recovers earlier. This could be expected naturally, without any complicated physics, if the line which fades earlier was intrinsically much fainter outside the minimum. However, this is not the case – [Ne III] is much stronger, having reached EW ∼ 5500 mÅ in early 2001 (close to the middle of the high-excitation phase) as compared to [Fe III], which maximum was EW ∼ 2800 mÅ. The intermediate-excitation energy lines [S III] and [Ar III] fall in between the two extremes, indicating that the order of fading and recovering is strongly modulated by the ionization potential (IP).

Fig. 2 indicates that also [S III] and [Ar III] follow the order *the line which fades earlier recovers later*. This is reinforced by the fact that [S III] reaches the zero intensity 0.5 d before [Ar III], as seen in column 2 in Table 2. However, this is the opposite to the trend *the higher the energy of the transition, the earlier the line fades*, although we note that the IPs of the two species are very similar. We cannot be sure that the two lines behave anomalously, or if this is just due to the quality of our data. On the one hand, the determination of the time to reach the zero intensity has an uncertainty of ∼1 d. On the other hand, the difference between the EWs of the two lines also is of the order of the errors. In addition, [S III] is seated on top of a variable broad Fe II line and the nearby stellar continuum is difficult to assess, and thus systematic effects may contaminate the measurements of this particular line.

Since the doubly ionized forbidden lines have different IPs and critical densities, we examined their correlation with the time to attain zero intensity (relative to $\phi = 0$). The time of zero intensity was derived in the same way as in paper I for the narrow component of He I λ6678: a linear fit through the descending branch of the line intensity curve extrapolated to zero. In the second column of Table 2, we display the time delays for several spectral features, with have a typical uncertainty of ∼1 d. We are focused on the first six lines in Table 1, formed in the Weigelt objects. Since the forbidden lines are collisionaly excited, we list the IPs to get the ion yielding the observed transition [i.e. IP(Ne^+) for Ne III], but as lines from He I are generally formed by recombination we give its IP. We see in column 2 of Table 2 that the time delay for disappearance has a general trend with the IP in the sense the higher the energy earlier the line fades as seen in Fig. 2. As shown in that table (column 4), the time delay is not correlated with the critical density for line formation.

The narrow nebular lines are known to originate around the dense Weigelt objects. If the radiation ionizing these blobs is suddenly extinguished, the line intensities will decay on a recombination time-scale. For He I, with $\alpha_B = 2.73 \times 10^{-13}$ at 10 000 K (Osterbrock 1989), the recombination time-scale is

$$t_{\rm rec} = 42.4 \left(\frac{10^6\ {\rm cm}^{-3}}{N_{\rm e}} \right)\ {\rm d},$$

where $N_{\rm e}$ is the electron density. Since He I decays on a time-scale of the order of 5–10 d, the density in Weigelt objects must, conservatively, exceed 10^6 cm^{-3}. Higher densities are possible, since it is likely that the line variations are also governed by the time-scale associated with the reduction in ionizing flux, which in turn is

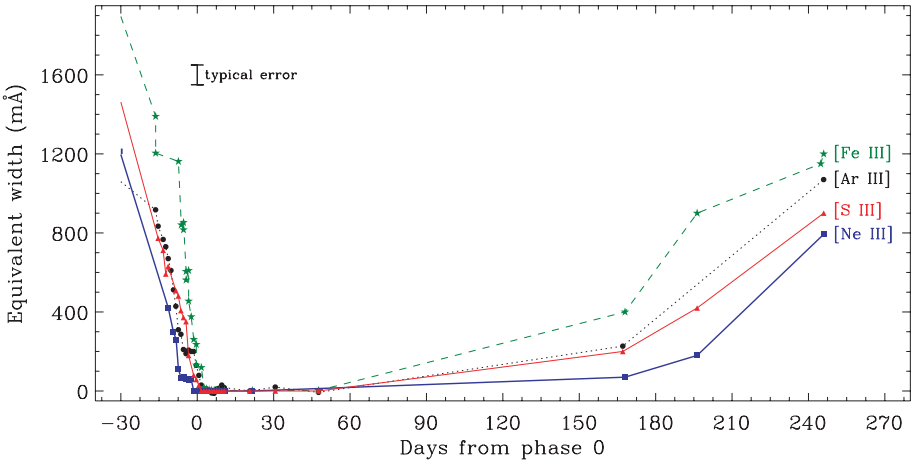

Figure 2. The central part of the minimum for the narrow components of the high-excitation lines. [Ne III] (squares), [Fe III] (stars), Ar III] (circles), [Si III] (triangles). [Ne III] has the highest transition energy, fading earlier and recovering later. [Fe III] has the lowest energy, fading later and recovering earlier. Ar III] and [Si III] have intermediate energy. The doubly ionized lines take at least nine months to recover the intensity they had a month before phase 0. Typical error bar is shown at the upper left of the figure.

Table 2. Time-delay to $\phi = 0$ for several features.

Feature pass-band	Time-delay (d)	IP (eV)	ρ_{crit} (cm^{-3})
[Ne III] λ3868	−5	41.0	7.6×10^6
[Ar III] λ7135	+2	27.6	5×10^6
He I λ6678 narrow line component	0	24.6	–
[S III] λ6312	+1.5	23.3	15×10^6
[Fe III] λ4701	+3	16.2	–
[N II] λ5754	+3.5	14.5	8.6×10^3
X-rays	−1	–	–
He II	+4	54.4	–
V band	+20	–	–
J band	+21	–	–
H band	+15	–	–
K band	+19	–	–
L band	+12	–	–
Radio 7 mm	+29	–	–
Paγ	(+1)	13.6	–

associated with the orbital time-scale around $\phi = 0$. The lower limit to the electron density is consistent with that given by Verner et al. (2005) who found $N_e \sim 10^7$ cm^{-3} for the high-ionization region from an analysis of Weigelt line ratios. It is consistent also with the results reported by Hartman et al. (2005) for the H II zones of the Weigelt objects.

The variation in other line intensities could also be used to place constraints on the density in the Weigelt objects. Hydrogen has a similar recombination time-scale to He I, while elements, such as N have a time-scale a factor of a few shorter. On the other hand, elements such as O (whose IPs are nearly the same as H), are coupled to the H by strong charge exchange reactions, and thus their recombination time-scale is determined by H.

For a simple spherical ionization bounded nebula, the ionization time-scale is similar to the recombination time-scale (Spitzer 1978). As the observed recovery in line strengths takes considerably longer than the decline, the variation in the obscuration of the ionizing source by intervening gas must be the primary factor determining the recovery time.

5.4 The *collapse* component in He I narrow emission lines

In Fig. 3(a), we present the EWs of the He I λ6678 narrow line component along the last three events. The label of the events are the same as in Paper I, in order that #9 has phase 0 on 1992.42, #10 on 1997.95 and #11 on 2003.49. There are two remarkable features in the *collapse* component of this line: (i) it is asymmetric and (ii) the post-minimum branch has been recovering at slower pace as time goes by. Both behaviours could be due to changes intrinsic to the line emission region, or just to a temporal increase in the level of the stellar continuum. If we demonstrate that changes in the stellar continuum across the *collapse* component are not the cause of the asymmetry, then the secular weakening of the recovering branch is also not due to brightening of the central source. The *collapse* component is a local feature, insensitive to temporal variations in the stellar continuum flux, which occur on longer time-scales.

In order to correct for possible changes in the stellar continuum across the minimum, we used published photometry to derive line fluxes for the He I λ6678 narrow line component along the event #11. Here, we are not interested in the absolute fluxes, only in the relative variations across the core of the event (*collapse* component). In this way, we normalized all quantities to the value they had on JD 245 2714 (represented by stars in Fig. 3b). The relative line flux is obtained by multiplying the relative flux nearby continuum by EW.

Variations in the continuum flux are easily derived from existing photometry, since we need only relative changes, avoiding complications involved in magnitude standardization. Color variations along the event are negligible in the optical window (at wavelengths longer than the Balmer jump), as indicated by the $B - V$ colour index (Lajús et al. 2003; van Genderen et al. 2003). The problem is that the amplitude of the variations depends on the aperture used to extract the magnitudes, and the ones of published photometry do not match the slit aperture used to record the spectra. The slit apertures encompass a few arcsecond (1.5–4 arcsec), as compared to ∼22 arcsec used in ground-based photometry. Although space-based photometry is available, the extraction apertures (0.3 arcsec) are much smaller than the slit widths. Since the slit width is intermediate to these two data sets, we can use them to constrain the flux variability.

The adoption of ground-based photometry would smear out the variations in the central star, since the extraction aperture

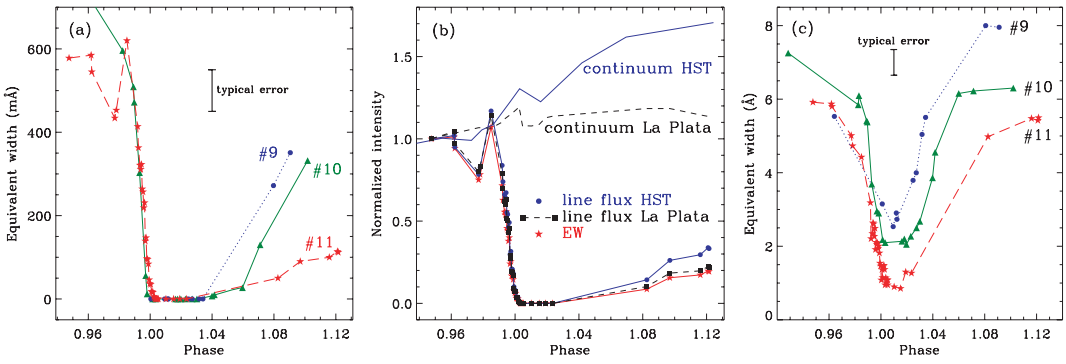

Figure 3. He I λ6678 line. Panel (a): EW of the narrow component in the last three events #9 (*circles*), #10 (*triangles*) and #11 (*stars*). Panel (b): normalized quantities for event #11: continuum of the central star from the STIS/*HST* HRC *F550M* filter (upper solid curve); *V*-band continuum of the Homunculus plus central star from La Plata photometry (dashed curve); narrow component line flux normalized with the (*HST*) stellar continuum (circles); narrow line components normalized with the Homunculus continuum (squares); normalized EW of the narrow line component (stars). (c) The same as panel (a), but for the broad component. Typical error bars for the line measurements are shown in the upper middle part of panels (a) and (c). Photometric errors are smaller than the widths of the lines.

encompasses the whole Homunculus nebula, which is bright in the optical region. The line flux variations obtained in this way are a lower limit to the one sampled by the slit width. In Fig. 3(b) (dashed line), we show flux variations derived from photometry taken at La Plata (Lajús et al. 2003). The magnitude is $V \sim 5$ and the errors are ∼0.005 mag, in order that they are a little larger than the width of the dashed line. We used the *V*-band measurements, since the *R* band is contaminated by Hα. The mismatch in wavelength between the line and the continuum is not important, since we are dealing with relative fluxes and the colour variations involving these two filters are very small. Relative fluxes in the *V*-band continuum, used to calibrate the line flux are presented by a dashed line at the upper part of the figure, are labelled as 'continuum La Plata'.

We can obtain an upper limit to the flux variations by using photometry from the central star, free from nebular contamination, as reported by Martin et al. (2006b) in their table 5. Those authors report synthetic photometry derived from *HST* STIS imaging through the medium-band HRC *F550M* filter. The magnitude for the event #11 was ∼6.5 with errors smaller than 0.01 mag. Relative fluxes for the central star are presented as a solid line in the upper part of Fig. 3(b), labelled as 'continuum *HST*' and the corresponding line fluxes are displayed as the dots at the bottom of that figure. As in the case of ground-based photometry, errors are similar to the thickness of the line that represents the continuum flux. The real relative fluxes of the He I λ6678 narrow line component are intermediate between the ones derived from ground- and space-based photometry. Taking into account the errors, the asymmetry between the descending and ascending branches appears to be real, and not an artefact of variations in the stellar continuum. On the other hand, allowing for the continuum variation does weaken the trend that the recovery phase is changing from cycle to cycle. Frequent observations during the recover phase of cycle 12 may help to clarify the cycle-to-cycle variations.

5.5 The *collapse* component in the broad He I emission lines

In Fig. 3(c), we display the EW of the He I λ6678 broad line component across cycles #9, #10 and #11. This broad line component is thought to be formed in the inner regions of the system, since it requires a relatively high flux of energetic photons and high density. We do not know the exact location, but possible candidates are the walls of the WWC shock-cone and the inner wind of the primary star. We must keep in mind that the central object is seen under heavy circumstellar extinction ($A_V \sim 7$ mag) as compared to the Weigelt objects ($A_V \sim 0.5$), which are primarily affected only by interstellar extinction (Hillier et al. 2001). Variability in these two components need not be correlated.

The central part of the minimum in this broad He I line component shares some similarities with the narrow component, but there are also important differences. Large variability is confined to a relatively short time interval ($\phi = 0.99$–1.035 or ∼90 d), very similar to the X-ray minimum. The centre of the minimum ($\phi = 0.015$ or ∼30 d after $\phi = 0$) is also coincident with that in X-rays and occurs much earlier than in the *slow variation* component (∼140 d). The minimum in the He I λ6678 broad component is a little asymmetric, in the sense that the fading is faster than the recovering, but to a much smaller extent than for the narrow line formed in the Weigelt objects.

It is interesting to note that the broad emission never disappears, which could indicate that there is always some ionizing radiation from the secondary star illuminating the walls of the shock-cone. Alternatively, the residual broad emission could simply be 'intrinsic' emission from the primary wind. The fact that the broad He I component is formed near the centre of mass and never disappears, indicates that eclipses cannot be invoked to explain all phenomena. For this line the real cause of the fast drop is a crash in the structure of the WWC which may also affect the escape of high-energy photons. Observations by Stahl et al. (2005) show that the broad line components weaken simultaneously in the Homunculus South Pole (via reflected light). This rules out an eclipse (or 'cone eclipse') mechanism, since different directions are affected simultaneously. We thus favor a model in which there is a collapse and restoration of the wind shock-cone. A beautiful realization of this idea is shown in the 3D numerical simulation by (Okasaki 2008).

What is causing the changes in the WWC? The secondary star does not seem to be the culprit. The repeatability of the X-ray light curve (Corcoran 2005) is remarkable. Since the X-ray emission is dominated by its wind (with the primary wind playing the role of a wall) the companion must be a stable star. The change should be in the primary star. If its mass loss decreases, the WWC shock is shifted farther from the secondary star and the shock-cone aperture is enlarged. This would cause a decrease in the ionization and as a consequence a weakening of the He I broad line component.

The WWC should reorganize some time after periastron, and its signature could be present in our data. The fast recovery in the X-ray light curve and the He I broad component line intensity at approximately three months after $\phi = 0$ indicates that at that time, the WWC is already restored and that our line-of-sight is again inside the shock-cone opening. Three months thus provides an upper limit to the duration of the WWC crash since we cannot exclude the possibility that the recovery in the X-ray light curve and the He I broad component corresponds to the end of the 'cone eclipse' to our specific direction.

The 'collapse' component takes much longer to end for the Weigelt objects. The ionization/excitation in the Weigelt objects (narrow components in the high-ionization forbidden lines and in He I) takes more than nine months to reach the same level as it had a month before $\phi = 0$. This is possible since they are at a line-of-sight different from ours. More importantly, they are far from the central source and the external parts of the shock-cone are distorted as it rotates around the orbit. After the collapse, additional gas may be trapped for some time inside the shock-cone. The slow recovery seen in the radio light curve may be due to the same cause.

5.6 The *collapse* component in the P Cygni absorption lines

P Cygni absorption lines are important because they sample the gas in a narrow beam to our side of the emitting region. They change as the source moves in the binary orbit and/or because the absorbing material suffers changes in the degree of excitation. Many lines display these components, which are strongly variable across the minimum. However, changes from cycle to cycle have also been observed.

The P Cygni absorption component, that is lost in He I λ6678 due to a blend with [Ni II], appears clearly in He I λ7065 line (Fig. 4a).[1] It reaches EW ≈ 0.5 Å at approximately three months before $\phi = 0$ and decreases with time. Three weeks before $\phi = 0$ it starts increasing, reaching a new maximum around $\phi = 0$ and then it decreases up to complete disappearance ∼20 d after. While the P Cygni absorption must be produced by material between us and the primary star there is still a debate whether it is directly related to material in the WWC cone, or produced by the wind of the primary

[1] The narrow and the broad emission components of He I λ7065 display a behaviour very similar to He I λ6678.

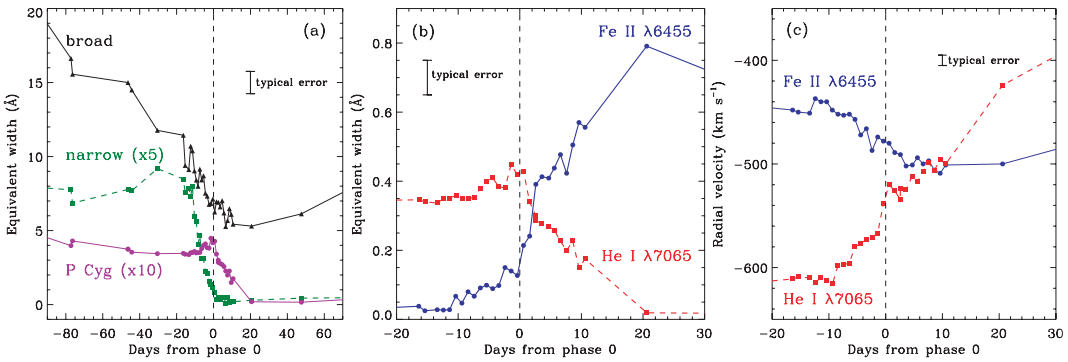

Figure 4. Panel (a): He I λ7065: EW of the broad emission (triangles); narrow emission component multiplied by 5 (squares); and the P Cygni absorption component multiplied by 10 (circles); panel (b): EW of He I λ7065 (squares)and Fe II λ6455 P Cygni absorption components (circles); panel (c): radial velocity of barycentre of He I λ7065 (squares) and Fe II λ6455 P Cygni absorption components (circles). Typical error bars are shown in the upper part of the panels.

(Nielsen, Ivarsson & Gull 2007b). For either scenario, the absence of P Cygni absorption during the minimum indicates that the aperture of the WWC cone is pointing away from us, which coincides with the position of the secondary star 'behind' the primary. With this orientation, He along our line-of-sight to the primary cannot be ionized by energetic photons from the secondary star. This gives support to the idea that the *collapse* component is produced by an 'eclipse-like' phenomenon that it is centred at approximately three weeks after $\phi = 0$.

The idea that the shock-cone is pointing away from us during the minimum is reinforced by comparing the P Cygni absorption component of He I λ7065 with that of Fe II λ6455. The large difference in excitation energy makes these two lines strategic to probe material at large and short distances from the ionizing source. In Fig. 4(b), we see that across the minimum, the absorption component in Fe II is rising while that of He I is fading, a behaviour also observed by Nielsen et al. (2007b) in *HST* spectra of the central source. The observed behaviour is a consequence of Fe II recombining on our side of the primary star wind, that is located on the opposite side of the primary star relative to the ionizing companion star. Just after the collapse, the wind of the primary star has recombined at maximum extent. It is interesting to see that the re-ionization (intensity decrease) of Fe II starts soon, as compared with the long absence of P Cygni absorption in He I. This behaviour of the He I P Cygni absorption component is expected, since the opening of the shock-cone takes time to point again to our direction. The re-ionization of Fe II in our side of the primary star wind, however, starts soon after the opposition of the secondary star, as its ionizing flux penetrates through the wind. The broad line component of He I λ6678 in Fig. 3(c) shows that the ionization recovers relatively quickly in the inner parts of the system, as compared to the slow recovery seen by the Weigelt objects.

The radial velocity of the P Cygni profile from these two lines provides an alternative way to analyze the situation just described. Fig. 4(c) shows the same opposite behaviour between He I λ7065 and Fe II λ6455 radial velocity as is shown by the line strengths. The Fe II λ6455 P Cygni absorption component shifts to more blueward velocities across $\phi = 0$, while the He I λ7065 P Cygni absorption component shifts to less blueward velocities. The amplitude of velocity changes is smaller in Fe II λ6455 because it is formed in regions where the wind is already reaching the terminal velocity as compared to He I that is formed in a zone subject to larger acceleration. The maximum speed of the He I λ7065 P Cygni absorption component (-610 km s^{-1}) is higher than that of the Fe II λ6455 P Cygni absorption component ($-500\,\mathrm{km\,s^{-1}}$). Since Fe II recombination occurs in regions where the primary star wind is reaching its terminal velocity, the He I line cannot be formed in the same stellar wind, as it requires higher excitation flux and gas density, only present close to the star. The only plausible formation regions for the He I broad line are the walls of the WWC shock-cone, not the primary's wind.

6 He I λ10830 Å – A PECULIAR SPECTRAL LINE

The He I λ10830 line is particularly interesting: it is very strong, displays many components in the central knot and in the nebular region, and undergoes remarkable variations. Fig. 5(a) displays the variability of the emission profile. It changes in intensity and width along the cycle. At high resolution, two peaks are clearly defined +12 (the 'R' peak) and $-85\,\mathrm{km\,s^{-1}}$ (the 'V' peak). The 'R' peak is higher than the 'V' peak (R/V $>$ 1) during the high-excitation state. The intensity ratio changes to R/V $<$ 1 at 105 d before $\phi = 0$ and again to R/V $>$ 1 at 4 d before $\phi = 0$ (Paper I). There is a question if the V and R peaks are independent emissions, or just a broad emission split into two by a shell absorption feature, as claimed by Damineli et al. (1998). Our present high-resolution spectra show that the putative 'shell absorption' does fall below the continuum only during the minimum. This is a false continuum, due to the depression of the local stellar continuum by the P Cygni absorption. The pseudo absorption profile remains steady at $-35\,\mathrm{km\,s^{-1}}$, as also the V and R peaks do. Although the radial velocity of the narrow absorption feature agrees with the faint absorption in Balmer lines, the R and V peaks vary independently and are steady in radial velcoity indicating separate emitting regions. The Weigelt objects are natural candidates for these two components, but the large separation in radial velocity ($97\,\mathrm{km\,s^{-1}}$) does not match that of the Weigelt objects. Moreover, when looking to long slit spectra, we see two narrow emission lines crossing all the field upt o the borders of the Homunculus. The two nebular lines are separated by $-127\,\mathrm{km\,s^{-1}}$, a little more than the R and V peaks. This happens because, in the central object, the nebular lines merge with the R and V peaks that are much broader and contaminated by the velocity field of the circumstellar gas.

Fig. 5(a) shows two additional emission peaks at -255 (V1 peak) and $-460\,\mathrm{km\,s^{-1}}$ (V2 peak). These two peaks are variable along the cycle and also from cycle to cycle. The absorption component at -1060 km s^{-1} (interstellar medium) was once believed to be a

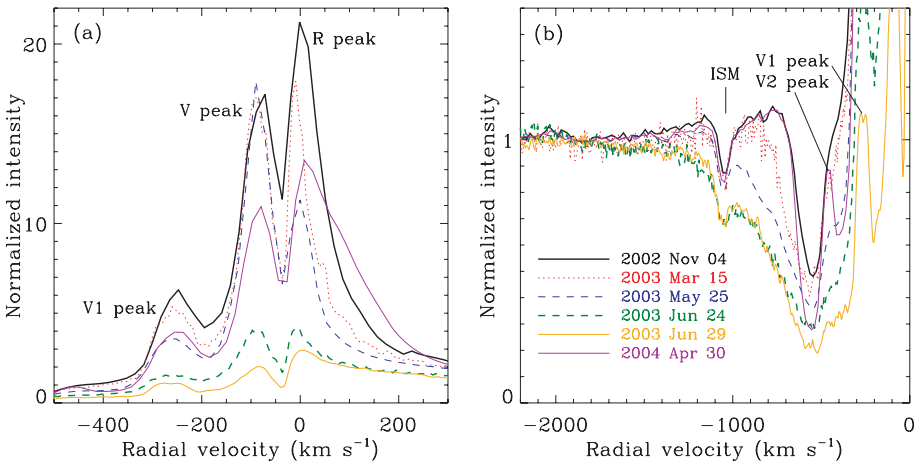

Figure 5. Line profile of He I λ10830. Panel (a): variability of the emission peaks (legend in panel b). Panel (b): zoom showing variations in the P Cygni absorption. Note the extension of the profile up to −1700 km s^{-1} near $\phi = 0$.

narrow absorption component in the stellar wind (Damineli et al. 1993), but Groh, Damineli & Jablonski (2007) showed that it is an interstellar/circumstellar feature. The P Cygni absorption during the high-excitation phase is faint and placed at −570 km s^{-1}, in agreement with the lines emitted by the wind of the primary star. As the minimum approaches, this feature starts to get broader and deeper, the centroid shifts up to −650 km s^{-1}. This change in the centroid is due to the contribution from the absorption wings that increases, extending up to −1400 km s^{-1}. When plotting together the spectra at maximum and minimum excitation, it is possible to track the line wings up to −1700 km s^{-1} While high velocities are generally not seen at our viewing angle, velocities of order 1000 km s^{-1} are seen from polar directions (Smith et al. 2003a). This led Smith et al. (2003a) to suggest that the wind of η Carinae is asymmetric, and that during the event a shell event occurs leading to a situation in which the equatorial wind more closely resembles the polar wind.

The P Cygni absorption component in He I λ10830 reaches its maximum strength (EW = 18 Å) 10 d after $\phi = 0$, a time when the absorption components in the optical He I lines have already faded. This could indicate that different spatial locations contribute to the observed absorption, although all absorbing structures must occur in gas between us and the primary. Surprisingly, the variability of the P Cygni line is more similar to the low excitation line Fe II λ6455 and that of He I λ7065. An alternative explanation for the distinct behaviour of the absorption component of He I λ10830 is related to the stability of the $2s^3S$ state. After the ionizing radiation field is switched off, the population of the metastable $2s^3S$ state will persist longer than the 2p states, which are the lower levels for the observed optical He I lines.

The radial velocity of the P Cygni absorption component in He I λ10830 has a behaviour similar to that of He I λ7065, with the minimum (maximum negative) velocity occurring ∼10 d before $\phi = 0$ and a maximum at ∼45 d after. The minimum speeds in He I λ10830 and He I λ7065 are −650 and −610 km s^{-1} and the maximum is −450 and −350 km s^{-1} respectively. The minimum (maximum negative) speed of the He I λ10830 P Cygni line is also larger than that of Fe II λ6455, indicating that it is not formed in the outer wind of the primary star. One possibility is that He I λ10830 forms in gas from the secondary star that has passed through the shock-cone, forming a tail left behind in a spiral-like pattern, as the secondary star turns around the centre of mass. When such portion of high-velocity gas ceases to be ionized by its parent star, it recombines, producing the extended wings in the P Cygni absorption.

The observed behaviour of the He I λ10830 emission profile is a combination of several effects. First, around the event, the Weigelt objects are shielded by the dense primary wind (and perhaps the star itself) from the ionizing radiation field, causing the narrow component to weaken, and disappear entirely during the state of minimum. Secondly, in order to explain the weakening of the broad component, the size of the He I emitting region must shrink near periastron. Since the number of ionizing photons emitted by the secondary star does not change during the event, why does the broad He I emission change? This must be due to the dense primary wind reprocessing the ionizing photons, and perhaps even the emitted He I photons. This in turn requires that the secondary star be deep within the primary wind at periastron. The residual broad He I emission, in both λ10830 and optical lines, that is observed during the minimum is probably produced by the primary. One possible caveat with this explanation is the weakness of the P Cygni absorption after the minimum. The calculations of Hillier et al. (2001) show that it is relatively easy to alter the strength of the intrinsic He I emission without significantly affecting H and Fe II line strengths, and thus this residual He I emission is easily explainable for reasonable luminous blue variable (LBV) parameters. One final feature that requires explanation is the high-velocity absorption profile seen during the minimum.

At minimum, the observed profile closely resembles that of HD 151804, which is an O8Iape (Groh et al. 2007). This must occur simply by chance, and cannot be the secondary star, since Hillier et al. (2006) showed that we would not expect to see the companion spectrum in the optical/IR, since the primary's luminosity is at least a few times higher than the secondary.

7 A MULTISPECTRAL VIEW OF THE MINIMUM

The spectroscopic events are present at all wavelengths – radio, IR, optical, UV and X-ray – and in spectral features such as the doubly ionized forbidden lines, the narrow He I lines, the broad He I lines, and the broad emission lines from the wind of the primary star. While all show the event, the characteristic behaviour varies

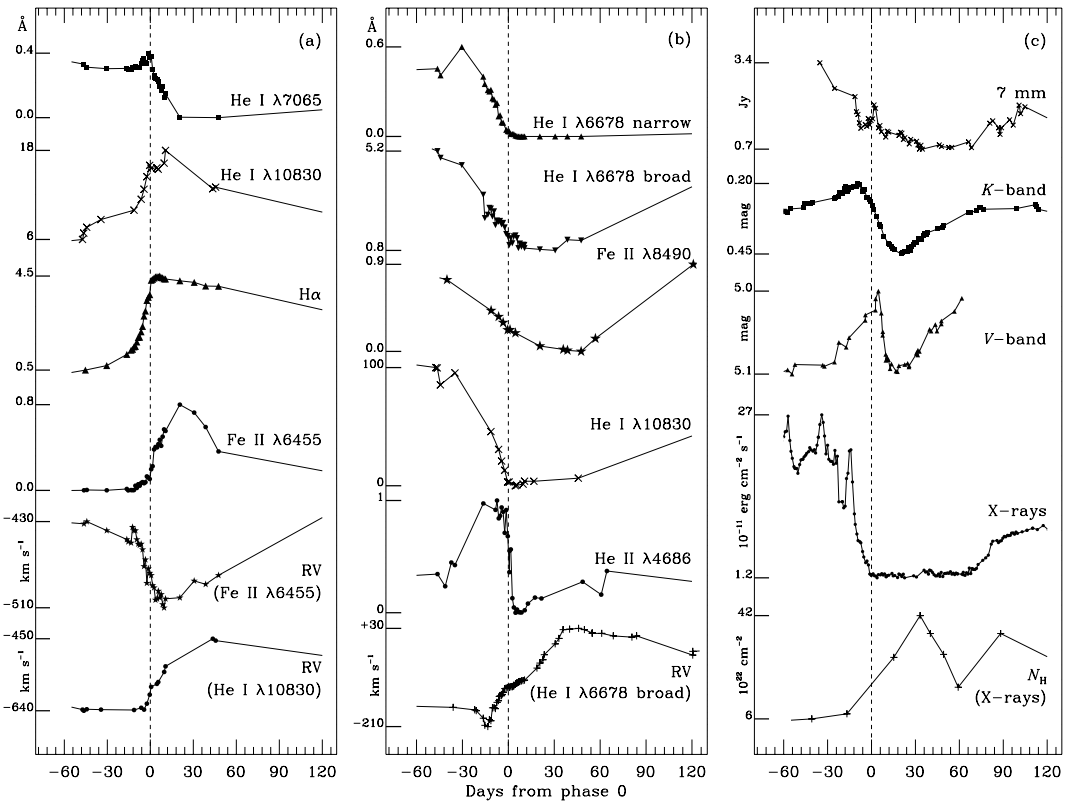

Figure 6. A panoramic view of variations in different features, and at different wavelengths, in the core of the event (*collapse* component). Panel (a): P Cyni absorption. EW in Å: He I λ7065; He I λ10830; Hα and Fe II λ6455 plus radial velocity of Fe II λ6455 and He I λ10830 in km s^{-1}. Panel (b): emission lines. EW in Å: He I λ6678 narrow and broad component; Fe II λ8490 (narrow) fluorescent line; He I λ10830 total line profile; He II λ4686 (Steiner & Damineli 2004); and radial velocity of He I λ6678 broad emission component in km s^{-1}. (c) Broad band. Radio 7-mm flux in Jansky (Abraham et al. 2005); *K*-band mag (Whitelock et al. 2004); *V*-band mag (Lajús et al. 2003); X-ray flux in 10^{22} erg cm^{-2} s^{-1} (Corcoran 2005); and X-ray column density ($N_{\rm H}$) in 10^{22} cm^{-2} (Hamaguchi et al. 2007).

dramatically. At one extreme, the radio 3-cm light curve shows only the *slow variation* and at the other extreme, He II and X-rays show only the *collapse* component. The observed behaviour rules out any mechanism for the event that works only close to periastron, such as a shell ejection around periastron (Martin et al. 2006a), accretion of the primary wind on to the secondary companion (Soker 2005) and eclipse of the shock-cone opening (Pittard & Corcoran 2002). Models like these, in which the minimum is produced only by geometrical factors ('cone eclipses'), are ruled out by radio observations.

In Fig. 6, we present a panoramic view of emission, absorption, radial velocity, and continuum flux variations across the minimum (collapse component), and across the spectrum. In addition to the measurements made in our spectra, we reproduce curves by other authors, taken from the cited literature. Here, we are not aiming to present full data, just the light curves morphology, to show the time of their maxima/minima and the decline/recovery phases. Since the plots are compressed in the Y scale, the errors are of the order of the size of the symbols.

We want to warn the reader that radial velocities presented were derived from the position of the centroid of broad lines. The line profiles are complex, and thus radial velocity variations do not represent the movement of some specific region. Our aim, by measuring centroids, was to produce robust model independent measurements. Variable and extended line wings introduce shifts in the centroids, not only in proportion to the wing extension, but to its intensity. In this work, we are not aiming to measure the full extent of the line wings, which is difficult because of their asymptotic merging with the stellar continuum. Such measurements would rely on subjective definition of the terminal speed, in addition to being limited by the S/N of the stellar continuum. Centroids represent the bulk of the velocity field.

The top four curves of Fig. 6(a) display the EW variation of P Cygni absorption features for four lines – each line shows its own unique variability curve. The EW of He I λ7065 P Cygni absorption is generally high along the 5.5-yr cycle, reaching a peak 2 d before $\phi = 0$. It then decreases with time, reaching the minimum 20 d after $\phi = 0$. In contrast, the EWs of the P Cygni absorption components of He I λ10830, Hα and Fe II λ6455 are low before $\phi = 0$, reach the maximum after that, and maintain a high intensity level for a relatively long time after $\phi = 0$. Hα reaches its maximum during the first week after $\phi = 0$ and seems to be saturated, decreasing very slowly after that. He I λ10830 reaches its maximum 10 d after $\phi = 0$, while Fe II λ6455 takes 20 d to reach its maximum.

The radial velocity variations in the Fe II λ6455 and He I λ10830 P Cygni absorption components are presented at the bottom of Fig. 6(a). We measured the position of the line centroid, by integrating along the absorption line profile, and so it corresponds to the barycenter of the P Cygni absorption component. Starting approximately two months before $\phi = 0$, Fe II λ6455 radial velocity shifts to higher (negative) values, reaching a minimum ∼10 d after $\phi = 0$ and returns to pre-minimum at a slower pace. The centroid of

the P Cygni absorption component shifts by ∼80 km s^{-1} across $\phi = 0$, indicating that the bulk of the recombination shifts toward larger radii. We have already shown that He I λ7065 P Cygni absorption moves in the opposite sense across $\phi = 0$, changing by 250 km s^{-1} in the time frame starting 10 d before $\phi = 0$ up to 50 d after it. The radial velocity of the He I λ10830 P Cygni absorption component behaves like He I λ7065. This seems confusing, since the intensity of this line behaves like Fe II λ6455. This can be explained if the He I λ10830 line has contributions from different regions, in the inner and outer parts of the system. The core of the P Cygni absorption in He I λ10830 seems to be formed close to that of He I λ7065, in the inner regions of the shock-cone and primary star wind. The wings of the P Cygni absorption, however, can be formed at larger distances, contributing substantially to the EW, but not too much to the radial velocity. We will discuss this point later in this paper.

We now turn our attention to emission-line strengths, displayed in Fig. 6(b). The He I λ6678 narrow component emission behaves like the doubly ionized forbidden lines that are emitted in the Weigelt objects; there is an extended minimum after $\phi = 0$ and a very slow recovery. The broad component of the same line shows a minimum at a later time and a faster recovery than the narrow component. A narrow fluorescent line, Fe II λ8490, shows a minimum at an even later time, but the general appearance of the *collapse* component is very similar to that of the He I λ6678 broad component. The EW of the complex He I λ10830 line displays a behaviour intermediate between that of the narrow and the broad components of He I λ6678, indicating that its emission-line profile is composed of both narrow and broad components.

The He II λ4686 line intensity curve is taken from Steiner & Damineli (2004). This line remains absent from the spectrum most of the cycle (Steiner & Damineli 2004; Martin et al. 2006a), rises quickly the month before $\phi = 0$ and displays a very sharp decline after that. The same behaviour was reported by Stahl et al. (2005) in the central star and reflected by dust in the pole of the Homunculus south-eastern lobe: at 2.6 arcsec south and 2.8 arcsec east from the star. A narrowing of the shock-cone, as in the case of X-rays, could explain the disappearance of He II from our line-of-sight and simultaneously (after correcting for the light travel time) from the Homunculus south-eastern pole, as long as the cone opening is pointing away from us at periastron, in agreement with other observations. Steiner & Damineli (2004) argued that He II λ4686 was excited by X-rays from the WWC, but Martin et al. (2006a) argued that this mechanism was too inefficient, and instead invoked a mechanism related to UV radiation from the central source although the precise details are unclear. The simultaneous disappearance from multiple viewing angles plus the strongly asymmetrical light curve suggest that He II 4686 emission is not simply a result of UV excitation in the inner wind of the secondary star, but instead might somehow be coupled to the WWC whose shape is strongly affected around periastron.

At the bottom of Fig. 6(b) we present the radial velocity curve of the He I λ6678 broad emission component. It shows a minimum of ∼−210 km s^{-1} at approximately two weeks before $\phi = 0$, a maximum (30 km s^{-1}) in coincidence with the middle of the X-ray minimum and then a slow decrease along the rest of the 5.5-yr cycle.

Fig. 6(c) shows measurements in the broad continuum bands. The light curve at 7-mm radio wavelength was made with data from Abraham et al. (2005). It is interesting, since the shape of the minimum is between that of long radio wavelength (3 cm), which varies slowly along the whole cycle and the of X-ray light curve, which has a very sharp minimum. The middle of the radio-mm minimum occurs approximately two weeks after that in X-rays.

The light curve in the *K* band was taken from Whitelock et al. (2004) and the *V* band from Lajús et al. (2003). The centre of the minimum in the *V* and *K* bands occur approximately two weeks before that in X-rays. Further, the duration of the minimum in these two photometric bands is the shortest among all the measured features. Both of them show a peak preceding the minimum, as discussed by Whitelock et al. (2004), and in both cases the variability amplitude is small ($\Delta V = 0.1$, $\Delta K = 0.25$).

The variation of $N_{\rm H}$, in units of 10^{22} cm^{-2} and reported by Corcoran (2005), is presented at the bottom of panel 6c. It behaves similarly to the Fe II λ6455 P Cygni absorption. It is important to notice that the time of maximum in these two features coincides with the middle of the X-ray minimum. We suggest that this time corresponds to the periastron passage. There is a secondary peak at approximately three months after $\phi = 0$, but we do not know if it is real, or just an unreliable measurement. Hamaguchi et al. (2007) show that the temperature of the WWC remains constant through the minimum, in contrast to the behaviour expected if the shock cools and collapses. However, Corcoran (2005) and Hamaguchi et al. (2007) show that there is a reduction in the emission measure during the minimum, which means that almost all of the WWC is hidden behind a very thick absorber. There is also some indication from the X-ray line profiles for a significant change in the physical condition in the WWC. One possibility would be that the shock-cone narrows significantly, in order that X-rays escape only to some defined direction. In this way, the X-ray light curve is modulated by both intrinsic and extrinsic (geometrical) causes.

In Fig. 7, we present radial velocity curves for broad lines covering a wide range of excitation energy: the broad emission lines of Si XIII–XIV – taken form Henley et al. (2008), He II λ4686 – taken from Steiner & Damineli (2004), He I λ6678 and H I λ10938 and the He Iλ7065 absorption, measured by us. Si II λ6347 broad emission

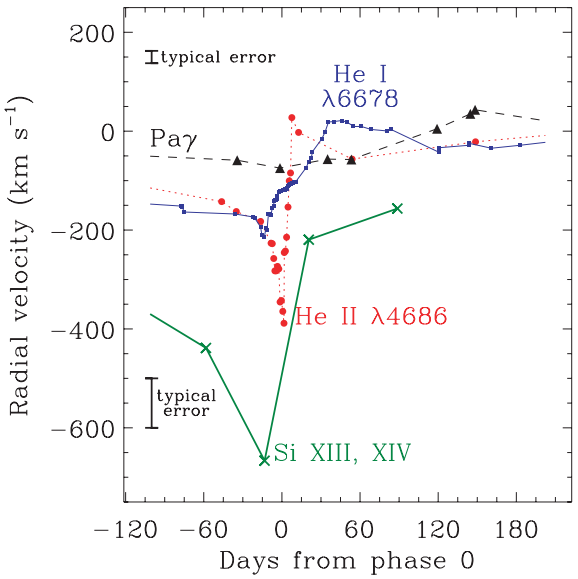

Figure 7. Radial velocity curves of broad emission lines close to $\phi = 0$, covering a wide range of excitation energies. Si XIII–XIV lines were averaged from data reported by Henley et al. (2008) and He IIλ4686 was taken from Steiner & Damineli (2004). Typical error bars for the optical/IR lines are in the upper part of the figure and for the combined X-ray lines at the bottom left-hand part.

and P Cygni absorption behave like He I (not shown here). We see a common signature of a slow shift toward higher negative speeds when approaching $\phi = 0$, then a sudden reversal to the positive side, followed by a new slow decrease towards the negative side. The extreme observed radial velocities are -700 km s^{-1} for the X-ray Si XIII–XIV lines (Henley et al. 2008), ~ -400 km s^{-1} for He II, ~ -200 km s^{-1} for He I and ~ -80 km s^{-1} for H I. The higher the excitation energy, the higher is the velocity jump at $\phi = 0$. Although the radial velocity changes are due to binarity, they do not track the orbital motion of the companion stars. Henley et al. (2008) were able to fit the X-ray lines if they are formed in the WWC cone walls.

Could the lower excitation lines presented in Fig 7 be interpreted in the same way as X-ray lines, since they share similar properties? He II λ4686, for example, is believed to be formed close to the X-ray emitting region (Steiner & Damineli 2004; Martin et al. 2006a). However, it is formed at lower temperatures than X-ray lines, which means farther from the apex than X-ray lines. Since the gas speed increases as it flows away from the cone apex, the lower excitation lines should have higher speeds, contrary to that is observed. The fact that the P Cygni absorption in He I λ7065 follows the same general pattern as very high energy emission lines is even more difficult to understand. One possibility is that, far from the apex, the conical surface does not exist anymore or it is dominated by large disturbed cells.

8 DISCUSSION AND CONCLUSIONS

From an analysis of the narrow components of forbidden emission lines we infer that the event is composed of two parts: the *slow variation*, and the *collapse* components. The former comprises almost the entire 5.5-yr cycle, is centred at a later time than the *collapse* component and the fading/recovering branches have a smaller degree of asymmetry. These lines are formed in the Weigelt objects and represent the way they 'see' the ionizing source, which is the radiation field of the secondary star that escapes through the shock-cone opening. The gentle fading and recovery indicates that the cone is not completely transparent. The obscuration of the ionizing source, as seen from the Weigelt objects, increases and decreases as the secondary star travels around the orbit and deep into and out of the primary's wind. The *slow variation* component indicates that the shape and gas density inside the shock-cone change along the cycle. Models invoking a shell ejection, accretion on to the secondary companion, or a simple eclipse by the primary, are unable to explain the *slow variation* component.

The *collapse* component is seen in many spectral features – X-rays, high-excitation Weigelt lines, He I P Cgyni absorption, and He I emission. It is likely that multiple processes are affecting the collapse phase, with its duration ultimately set by the amount of time the companion spends near periastron in its highly eccentric orbit. Eclipse-like effects ('cone eclipse') could produce a decrease in lines formed in the Weigelt objects, in the inner system and reflected in the dusty Homunculus and features. However, not all directions can be affected at the same time.

Due to uncertainties in the orbital and stellar parameters it is unclear how close the primary and secondary stars approach at periastron. However, because of the much higher densities near periastron, and the rapidly changing orbit, conditions in the shock-cone will change, and it is possible that instabilities will occur. The observed behaviour of many spectral features might be explained by a global disruption of the WWC shock. With this model it is also easy to explain the observed asymmetry seen in the *collapse* light curves around minimum. The bow shock is not symmetrically orientated around periastron and its structure is not identical either side of periastron. In addition to the Coriolis effect, the companion stars are approaching each other before periastron and receding after, changing the relative speeds at which the winds collide.

Although we could not identify unambiguously the signature of the WWC restoration, it must happen at most three months later than $\phi = 0$. At three months, their is the sharp recovery in the intensity of X-rays and the He I broad emission lines. This is either due to the restoration of the WWC, or due to the end of the 'cone eclipse' (in which case the restoration of the shock must have occurred earlier).

The doubly ionized forbidden lines show a remarkable behaviour in the *collapse* component. There is a trend of the time delay of line fading with the IP, indicating that the Weigelt objects see an ionizing spectrum that becomes progressively softer as the minimum is approached, and progressively harder in the recovery phase. This must be caused by optical depth effects of intervening gas in between the ionizing source and the blobs. The slow re-ionization of the blobs (more than six months after the minimum for [Ne III]) is most likely due to obscuration effects. Since the line intensity curves of the high-energy forbidden lines do not flatten out in the high-excitation state, it is probable that only a fraction of the gas in the Weigelt objects is ionized to Ne^{++}, S^{++} and Ar^{++}.

Very high energy features, such as X-rays and He II λ4686, display almost only the *collapse* component. Conversely, at radio cm wavelengths the light curve is dominated by the *slow variation* component. At millimetre wavelengths, the *collapse* component is present at a modest level.

The minimum of the radio 7-mm light curve is centred at ∼42d after $\phi = 0$. Although the WWC shock may be responsible for a fraction of the radio emission at these energies, most of the emission comes from ionization in the gas outside the binary system. Some effects, such as the light travel time from the source and recombination time of the gas, can represent a delay to the centre of the minimum in order that this epoch is compatible with the centre of minimum in X-rays.

He I P Cygni absorption (and broad emission) lines cannot be formed in the wind of the primary star, since its speed reaches values larger than those of P Cygni absorption in Fe II λ6455, which is formed in the external layers of the primary's wind.

As the P Cygni absorption component of Fe II λ6455 reaches the maximum intensity and maximum negative velocity approximately three weeks after $\phi = 0$. the wind of the primary star is recombined to a maximum extent at that time. It must occur when the (ionizing) secondary star is at opposition. This interpretation is corroborated by the fact that around $\phi = 0$ the velocity of the P Cygni absorption component of Fe II λ6455 is shifting to the negative side, and that of He I λ7065 P Cygni absorption to the opposite direction. Other features associated with the shock-cone of the secondary star support this scenario, such as the He I λ6678 broad emission component that also is shifting to the positive side of radial velocities and reaches the minimum at $\phi = 0.01$. The X-ray flux reaches a minimum and the column density ($N_{\rm H}$) reaches a peak 30 d after $\phi = 0$. Moreover, the fluorescent (narrow) line Fe II λ8490 also reaches a minimum around $\phi = 0.015$. These data, taken together, indicate that the opposition of the secondary star occurs 20–30 d after $\phi = 0$. We do not claim that this is an eclipse in a classical sense, neither from the primary stellar disc nor from its wind.

The He I λ10830 line indicates that material along our line-of-sight latitude reaches much higher negative velocities (-1400 km s^{-1}) than the typical velocities we see in the

high-excitation phases (-550 km s^{-1}). Most likely the P Cygni absorption is due to secondary gas that flows through the walls of the shock-cone and is left behind as the secondary star turns around the centre of mass at periastron. Variations in the V and R line peaks indicate that there are other emitting regions for this spectral line, in addition to the Weigelt objects and the winds of the companion stars.

Although the observations reported here are compatible with the generic binary scenario presented in Section 4, none of the existing models describes the whole data set. A numerical 3D simulation of two-colliding winds for parameters appropriate to the η Carinae system will be needed to assist in understanding the complex variability that is observed. Work in progress (Okasaki 2008) is very promising, having been able to reproduce the near-periastron collapse, compatible with data we presented here.

If we are to understand η Carinae and its evolutionary state, the identification of genuine Keplerian velocity-shifts, and the determination of the masses and spectral types of both stars, is a crucial goal. The intensive efforts applied to understand η Carinae, which is a difficult system because of extreme conditions (masses, mass-loss, orbital eccentricity), bring benefits to the field of colliding wind binaries. Binarity in η Carinae may not have been responsible for the 1843 giant eruption, and so does not explain the other examples of extreme LBVs, like P Cygni, V1 in N2363, etc. However, the secondary star in η Carinae probes different regions of the primary's wind and, hopefully, will enable the determination of its mass. This is helpful in understanding the parameters of evolved massive stars, which are difficult to diagnose when in isolation.

The next minimum is predicted to start on 2009 January 11 ($\pm$2 d). Fig. 6 is useful to plan monitoring campaigns through the *collapse* component. The time frame starts in early 2008 November and extends through 2009 July. This is the best event since 1948 for ground-based observations, since its central core fits entirely in the good observing season. The next favorable event will not occur before 2020. The critical time for narrow components of the high-excitation lines and He I encompasses the time interval December 15 to January 20. The P Cygni absorption and the $N_{\rm H}$ to the X-ray source will reach the maximum around February 10. In order to improve significantly the observations made in the 2003.49 event, it is necessary to monitor this critical time interval more frequently than one observation per day.

Since we now have a better picture of the events, we can plan for the next critical observations focused on a few representative lines. Major gains, relative to the present knowledge, will come from higher spatial resolution and S/N observations. Signatures from high-energy phenomena, like X-rays, He II λ4686 and the Balmer jump are especially important.

ACKNOWLEDGMENTS

We thank J. E. Steiner, T. Gull and N. Soker for their comments on this draft. AD, JHG and MT thank FAPESP and CNPq for continuing support. JA is supported by Fondo ALMA para el desarrollo de la Astronomía, CONICYT No. 31050004.

REFERENCES

Abraham Z., Falçeta-Gonçalves D., Dominici T. P., Nyman L.-Å., Dourouchoux P., McAulaife F., Caproni A., Jatenco-Pereira V., 2005, A&A, 437, 977
Corcoran M. F., 2005, AJ, 129, 2018
Damineli A., 1996, ApJ, 460, L49
Damineli A., Viotti R., Baratta G. B., de Araújo F. X., 1993, A&A, 268, 183
Damineli A., Conti P. S., Lopes D. F., 1997, New Astron., 2, 107
Damineli A., Stahl O., Kaufer A., Wolf B., Quast G., Lopes D. F., 1998, A&AS, 133, 299
Damineli A., Stahl O., Wolf B., Kaufer A., Jablosnki F. J., 1999, in Morse J. A., Humphreys R., Damineli A., eds, ASP Conf. Ser. Vol. 179, eta Carinae at the Millennium. Astron. Soc. Pac., San Francisco, p. 221
Damineli A., Kaufer A., Wolf B., Stahl O., Lopes D. F., de Araújo F. X., 2000, ApJ, 528, L101
Damineli A. et al. 2008, MNRAS, 384, 1649 (Paper I)
Davidson K., 2002, in Schlegel E. M., Vrtilek S. D., eds, ASP Conf. Ser. Vol. 262, The High Energy Universe at Sharp Focus. Astron. Soc. Pac., San Francisco, p. 267
Davidson K., Ebbets D., Weigelt G., Humphreys R. M., Hajian A. R., Walborn N. R., Rosa M., 1995, ApJ, 109, 1784
Davidson K. et al., 1999, AJ, 118, 1777
Davidson K. et al., 2005, AJ, 129, 900
Dorland B. N., Currie D. G., Hajian A. R., 2004, AJ, 127, 1052
Duncan R. A., White S. M., 2003, MNRAS, 338, 425
Duncan R. A., White S. M., Lim J., 1997, MNRAS, 290, 680
Feast M., Whitelock P., Marang F., 2001, MNRAS, 322, 741
Gaviola E., 1953, ApJ, 118, 234
Groh J. H., Damineli A., 2004, IBVS 5492
Groh J. H., Damineli A., Jablonski F. J., 2007, A&A 465, 993
Hamaguchi K. et al., 2007, ApJ, 663, 522
Hartman H., Damineli A., Johansson S., Letokhov V. S., 2005, A&A, 436, 945
Henley D. B., Corcoran M. F., Pittard J. M., Stevens I. R., Hamaguchi K., Gull T. R., 2008, preprint (arXiv:0801.4779)
Hillier D. J., Allen D. A., 1992, A&A, 262, 153
Hillier D. J., Crowther P. A., Najarro F., Fullerton A. W., 1998, A&A, 340, 483
Hillier D. J., Davidson K., Ishibashi K., Gull T., 2001, ApJ, 553, 837
Hillier D. J. et al., 2006, ApJ, 642, 1098
Humphreys R. M., Koppelman M., 2005, in Humphreys R. M., Stankek K. Z., eds, ASP Conf. Ser. Vol. 332, The Fate of the Most Massive Stars. Astron. Soc. Pac., San Francisco, p. 159
Ishibashi K., Corcoran M. F., Davidson K., Swank J. H., Peter R., Drake S. A., Damineli A., Whithe S., 1999, ApJ, 524, 983
Ishibashi K., Gull T. R., Davidson K. et al., 2003, AJ, 125, 3222
Kashi A., Soker N., 2007, New Astron., 12, 590
Lajús E. F., Gamen R., Schwartz M., Salerno N., Llinares C., Fariña C., Amorín R., Niemela V., 2003, IBVS 5477
Martin J. C., Koppelman M. D., 2004, AJ, 127, 2352
Martin J. C., Davidson K., Humphreys R. M., Hillier J. D., Ishibashi K., 2006a, ApJ, 640, 474
Martin J. C., Davidson K., Koppelman M. D., 2006b, AJ, 132, 2717
Nielsen K. E., Corcoran M. F., Gull T. R., Hillier D. J., Hamaguchi K., Ivarsson S., Lindler D. J., 2007a, ApJ, 660, 669
Nielsen K. E., Ivarsson S., Gull T. R., 2007b, ApJS, 168, 289
Okasaki A., 2008, http://www.arc.hokkai-s-u.ac.jp/okazaki/index-e.html
Osterbrock D., Ferland G. J., 2006, Astrophysics of Gaseous Nebulae. University Science Books, Mill Valley, CA
Pittard J. M., Corcoran M. F., 2002, A&A, 383, 636
Smith N., Davidson K., Gull T. R., Kazunori I., Hilier J. D., 2003a, AJ, 586, 432
Smith N., Gehrz R. D., Hinz P. M., Hoffmann W. F., Hora J. L., Mamajek E. E., Meyer M. R., 2003b, AJ, 125, 1458
Smith N. et al., 2004, ApJ, 605, 405
Soker N., 2005, ApJ, 635, 540
Soker N., Behar E., 2006, ApJ, 652, 1563
Spitzer L., Jr, 1998, Physical Processes in the Interstellar Medium. Wiley-VCH, Berlin
Stahl O., Weis K., Bomans D. J., Davidson K., Gull T. R., Humphreys R. M., 2005, A&A, 435, 303
Steiner J. E., Damineli A., 2004, ApJ, 612, L133

Teodoro M., Damineli A., Sharp R. G., Groh J. H., Barbosa C. L. 2007, MNRAS, in press (arXiv:0804.0240)
van Genderen A. M., Sterken C., Allen W. H., Liller W., 2003, A&A, 412, L25
van Genderen A. M., Sterken C., Allen W. H., Walker W. S. G., 2006, JAD, 12, 3
Verner E. M., Gull T. R., Bruhweiler F., Johansson S., Ishibashi K., Davidson K., 2002, ApJ, 581, 1154
Verner E., Brhuhweiler F. B., Gull T. R., 2005, ApJ, 624, 973
Weigelt G., Ebersberger J., 1986, A&A, 163, L5
Weis K., Stahl O., Bomans D. J., Davidson K., Gull T. R., Humphreys R. M., 2005, AJ, 129, 1694
Whitelock P. A., Feast M. W., Marang F., Breedt E., 2004, MNRAS, 352, 447
Whitney C. A., 1952, Harvard College Observatory Bulletin No. 921, 8

This paper has been typeset from a TEX/LATEX file prepared by the author.